The 18th Nano Bio Info Chemistry Symposium

December 14-15, 2021

Overview: The 18th Nano Bio Info Chemistry Symposium will be held online, December 14-15, 2021.

Notice: Due to the outbreak of COVID-19 and for the safety of our participants, this symposium has been changed to Online Conference.

The online Symposium consists of two parts:

1) Oral Presentation with a pre-recorded video or real time presentation via Zoom
2) Discussion via Zoom

Organizers

The Chemical Society of Nano Bio Info
Physics Faculty of Orenburg State University

Co-organizers

The Chugoku Shikoku Branch, The Chemical Society of Japan
The Chugoku Shikoku Branch, The Society of Synthetic Organic Chemistry, Japan
The Chugoku Shikoku Branch, The Japan Society for Analytical Chemistry
The Chugoku Shikoku Branch, The Spectroscopical Society of Japan

Contributions

The Hiroshima Chemistry Alumni Association
Global Career Design Center, Hiroshima University

2021 December 14th Tuesday

Japan Time	Russian Time			
12:45:00	08:45:00	Online Site Open		
13:00:00	09:00:00	Opening Remark		
		Chairman: Goulven Cosquer		
13:05:00	09:05:00	1A1a	Bangun satrio nugroho Modulating the cesium adsorption performance by composing graphene oxide with dawson-type polyoxometalate	☆
13:25:00	09:25:00	1A2b	Savinov Vladislav Features of sedimentation of fine fraction of montmorillonite.	☆
13:40:00	09:40:00	1A3b	Akimova D. A. Products of the nisyros volcano eruption, greece	☆
13:55:00	09:55:00	Break		
		Chairman: Eskender Alidganov		
14:10:00	10:10:00	1B1b	Sadykov Alexander Suppression of spontaneous emission due to intra-atomic interference	☆
14:25:00	10:25:00	1B2b	Shimada Yuta Attempt to synthesize silyl-substituted diphophatetrahedrane: highly strained organophosphorus molecule	☆
14:40:00	10:40:00	1B3b	Kaepkulova Elina Noncollinear spin and magnetic structures due to hyperfine interactions	☆
14:55:00	10:55:00	Break		
		Chairman: Hike Nikiyan		
15:10:00	11:10:00	1C1b	Goda Ryosuke Conformation of crown ether complexes with alkylammonium ions and its dependence on alkyl chain length under cold gas-phase conditions	☆
15:25:00	11:25:00	1C2b	Dianova Yulia Production and study of the stability of suspensions of paraffin wax modified with polyethylene glycol	☆
15:40:00	11:40:00	1C3b	Doroshkevich A. V. Inactivation of bacteria in solutions by shock acoustic waves	☆
15:55:00	11:55:00			

IL: Invited Lecture (35 min including Q&A, Zoom)
a: Oral presentation a (20 min including Q&A, Zoom)
b: Oral presentation b (15 min including Q&A, Zoom)
☆: Candidate to the student and young scientist award

2021 December 15th Wednesday

Japan Time	Russian Time			
12:45:00	08:45:00	Online Site Open		
		Chairman: Shang Rong		
13:00:00	09:00:00	2A1a	Herry Wijayanto Cs desorption from clays and clay minerals by quaternary ammonium cations: the role of ammonium head group structures	☆
13:20:00	09:20:00	2A2b	Stepanov Artem Flame synthesis of carbon nanoparticles and study of their properties.	☆
13:35:00	09:35:00	2A3b	Hirokawa Yasuaki Development of cryogenic gas-phase spectrometer aiming for mechanistic study of metal cluster catalysts	☆
13:50:00	09:50:00	Break		
		Chairman: Berdinskiy Vitaly		
14:05:00	10:05:00	2B1b	Sokabeva Saniya Mechanism and nonlinear heating kinetics of titan oxide by microwaves	☆
14:20:00	10:20:00	2B2b	Takahashi Shusaku Development of metal nanoparticles doped nanographene	☆
14:35:00	10:35:00	2B3b	Yudin Alexander Definition of the chemical activity of silicon oxide nanoparticles	☆
14:50:00	10:50:00	Break		
		Chairman: Inoue Katsuya		
15:05:00	11:05:00	2IL	Muramatsu Satoru Cold gas-phase spectroscopy: a case study of hypervalent carbon compounds	
15:40:00	11:40:00		Closing of the Symposium	
16:00:00	12:00:00			

IL: Invited Lecture (35 min including Q&A, Zoom)
a: Oral presentation a (20 min including Q&A, Zoom)
b: Oral presentation b (15 min including Q&A, Zoom)
☆: Candidate to the student and young scientist award

1A1a

Modulating the Cesium adsorption performance by combining graphene oxide (GO) with Dawson-type Polyoxometalate

Bangun Satrio Nugroho,[1,2] Satoru Nakashima[1,2,3]

[1] Department of Chemistry, Graduate School of Science, Hiroshima University
[2] Radioactivity Environmental Protection Course, Phoenix Leader Education Program, Hiroshima University
[3] Natural Science Centre for Basic Research and Development, Hiroshima University

The complexity in the chemical structure of graphene oxide (GO) has potentially opened the unique properties specifically in cesium (Cs) adsorption character, where the C/O ratio of GO has a significant role. This work has produced a new GO-POM nanocomposite by combining GO which has a different C/O ratio with Dawson-type polyoxometalate (POM). The composites were characterized using PXRD pattern, Raman spectra, FTIR spectra, ICP-AES, TEM, and SEM imaging. The TEM and SEM imaging demonstrated that the Dawson-type POM successfully interacted above the surface of GO. In addition, small black spots were observed after the Cs adsorption. Moreover, the PXRD pattern, Raman spectra, and ICP-AES revealed that the Cs adsorption has occurred. It occurred by the aggregation process. The result revealed that the Cs adsorption capacity increased effectively by employing GO-POM nanocomposite compared to the original material (GO-only). The detail investigation showed that in the Cs adsorption process, the nanocomposite sample coagulated immediately after stirring and keeping the Cs-adsorbed sample in the ambient temperature. For GO which has C/O ratio 3.34-3.64 the brown milky coagulation was formed in high yield compared to the other GO which has C/O ratio 0.68-0.69. Based on SEM imaging, the small granule of Cs was formed. The PXRD pattern showed the fact that the sharp and the intense diffractions were significantly reduced after Cs adsorption. A similar tendency was also seen in the second-order peak of Raman spectra after Cs adsorption. Furthermore, the specific changes are marked at 1150 cm $^{-1}$-1350 cm^{-1} in FTIR spectra after the Cs adsorption process in all GO-POM nanocomposites. For nanocomposite consisting of ~39 wt % C element, the IR spectrum showed significant changes compared to the nanocomposite that consists of 70-72% C element. This suggested that there is a change in the interlayer chemistry of the samples. The interlayer distances were expanded in all nanocomposites after Cs adsorption. The present results revealed the three important points. First, the different C/O ratios of GO have played an important role in Cs adsorption performance after forming the GO-POM nanocomposite. The GO which has C/O ratio 3.34-3.61 is a good precursor material than GO which has C/O ratio 0.68-0.69 to incorporate Dawson-type POM. Second, to fully maximize the Cs adsorption performance, the ratio of GO/POM may become important, although the precise study is needed. Third, the size of GO and its composite are important in Cs adsorption performance, although the precise study is needed.

1A2b Features of sedimentation of fine fraction of montmorillonite.

Vladislav Savinov,[1,2]Olga Kanygina[1,]

[1] Department of Chemistry, Faculty of Chemistry and Biology, Orenburg University.
[2]Center for support of talented children of the Orenburg region "Gagarin", Russia

1. Introductions

The mineral montmorillonite finds its application in many industries, including in the field of nanotechnology, where nanodisperse fractions of montmorillonite are used as a filler for some nanocomposite materials[1].

Obtaining a nanodisperse fraction of montmorillonite is complicated by a number of problems.

Firstly, it is impossible to obtain a fraction containing exclusively nanoparticles by conventional mechanical dispersion, because as a result of grinding, a large range of diameters is formed, including particles of about 1 mm in size[2].

Secondly, the presence of a charge on the surface of the particles leads to their immediate adhesion and enlargement, which again complicates the task. This problem can be solved by covering the particles of montmorillonite with hydrate shells, i.e. transfer the particles to an aqueous medium. The surface charge will be compensated by water dipoles, and accordingly, the agglomeration of particles will decrease. The presence of particles in a suspension state can allow ultrasonic dispersion of particles to nanoscale. However, even with this method of particle preparation, it is not impossible to obtain nanoparticle sizes in a narrow range.

The paper[3] describes the model of an "imaginary" particle as a method for calculating the ratio of the mass of clay to the volume of suspension. However, in this paper, the experimental confirmation of the model is proved by the method of nephelometry, which does not fully characterize the particle size distribution depending on the concentration of clay, but only indirectly characterizes the change in the concentration of the colloidal system. It follows from this that it is necessary, along with the concentration of the resulting colloidal solution, to determine the particle sizes in it.

The purpose of the work: To determine by the method of dynamic light scattering the dependence of the size of sedimenting particles of montmorillonite clay on the concentration of the suspension.

2. Materials and methods

To determine the dependence of the size of the montmorillonite particles on the concentration of the suspension, a control sample with a mass of 1.2486 g per 150 ml of volume calculated by formula 1 was prepared:

$$\boldsymbol{m = \frac{V_c \bullet \rho \bullet k}{216}}, \qquad (1)$$

where *Vc* is the volume of the system;

p is the average density of the substance (g/cm3);

k is the swelling coefficient.

proposed in the work [3]. At the same time, a series of samples with a smaller and larger weight of the sample relative to the control sample was prepared. When creating the suspension, the samples were subjected to ultrasonic dispersion at a frequency of 30 kHz for 300 seconds.

Particle size control was carried out by the method of dynamic light scattering at a temperature of 20 ℃ on the device "Photocor mini" with subsequent processing of the correlation function of fluctuations in the intensity of light scattering.

As a result of the experiment, particle size ranges were determined for the clay concentration range from 0.67 to 15.04 g/l. After processing the correlation function, the dependence of the maximum particle sizes on the concentration of clay in water was constructed (Figure 1). On the graph, the control sample is marked at 8.3 g/l.

The processing of the correlation function also makes it possible to determine the fractions of particles of different sizes in the solution, to construct the dependences of the quantitative ratio of the hydrodynamic radii of particles on the concentration of the suspension.

The range of particle sizes can be estimated by describing the dependence of the fraction of particles of maximum and minimum size on the concentration of the suspension.

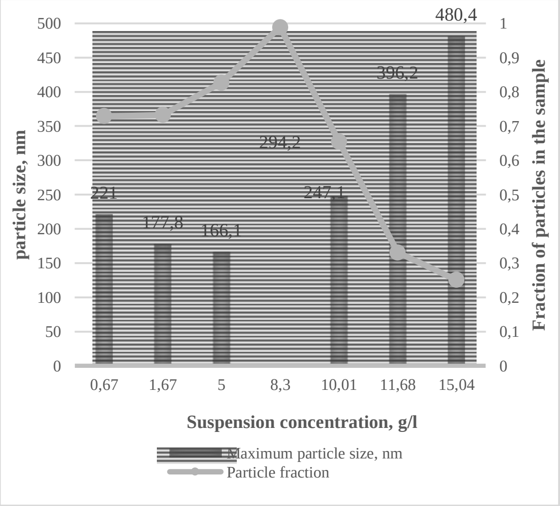

Figure 1 - The dependence of the maximum hydrodynamic radii of particles on the concentration of the suspension and their proportion in the sample.

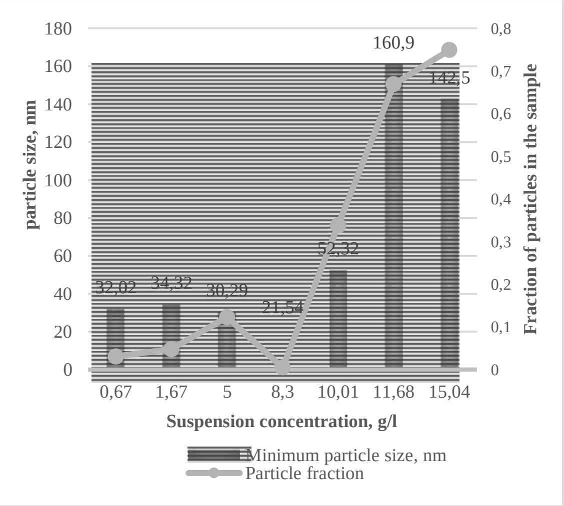

Figure 2 - The dependence of the minimum hydrodynamic radii of particles on the concentration of the suspension and their proportion in the sample.

The graph (Figure 1) shows two dependencies: the upper limit of the size of the hydrodynamic radius of particles on the concentration of the suspension and the proportion of these particles in the sample. After a control sample of 8.3 g/ l, a sharp enlargement of the particles is observed. The proportion of particles smaller than 500 nm reaches 99% in the control sample, and then, due to the fact that the particles begin to agglomerate, their number decreases to 25%.

Sharp coagulation appears when considering the lower limits of the size of the hydrodynamic radius of particles from the concentration of the suspension and their proportion in the sample. Active enlargement of small particles begins after the control sample at a concentration of 8.3 g/l (Figure 2).

The content of particles less than 100nm varies within 20%, but in the control sample their proportion is 0.5%. Then there is a sharp increase in the lower limit of the hydrodynamic radii of particles during their coagulation.

It is obvious that the weight of the sample calculated using the "imaginary" particle model is the limiting mass at which the phenomenon of coagulation begins to influence the ratio of dimensions of montmorillonite nanoparticles during sedimentation.

3.Conclusion

The optimal conditions for the concentration of nanoparticles under normal conditions are studied.

The maximum concentration of clay -8.3 g/l - in an aqueous-clay suspension was calculated, in which coagulation of montmorillonite nanoparticles was excluded by the sedimentation method of their isolation. The particle size range is about 270 nm (from 21 to 294 nm). This will allow the most productive synthesis of nanocomposite materials.

In the future, it is necessary to consider the effect of temperature on the concentration parameters of nanoparticles, taking into account the change in the rate of their coagulation

References

1 Uddin, F. Clays, Nanoclays, and Montmorillonite Minerals. Metall and Mat Trans. - A 39 / F. Uddin. – 2008. - P. 2804–2814.

2 Vaia, R. A. Interlayer structure and molecular environment of alkylammonium layered silicates / R. A. Vaia, R. K. Teukolsky, E. P. Giannelis, Ghem. Mater. - V.6. – 1994. - P. 1017-1026.

3 Savinov V. V. et al . The "imaginary particle" model as a method for describing sedimentation in highly dispersed clay water suspensions //The University complex as a regional center of education, science and culture. - 2020. - pp. 2299-2306.

PRODUCTS OF THE NISYROS VOLCANO ERUPTION, GREECE

AKIMOVA D. A.

Russia, Orenburg, Orenburg State University

daraakimova208@gmail.com

1A3b

Throughout the history of the Earth, volcanic eruptions have caused environmental and economic damage to the inhabitants of the Earth. The most impressive volcanic phenomena are the materials of the eruption in the form volcanic bombs, lappils and volcanic ash. The interest of researchers in volcanoes and the products of its activity is high, but little attention is paid to pyroclastic formations that affect the formation of the Earth's outer shells - the lithosphere, hydrosphere and atmosphere. Now there are about 90 active volcanoes on the Earth's surface, affecting the clima relief and chemical composition of soils, waters and living organisms.

The purpose of my research is to study the granulometric and chemical compositions of volcanic ash and volcanic rocks of the Nisyros volcano, samples of which were kindly provided by V.L. Berdinsky.

Methods of X-ray spectral analysis and optical microscopy using the ImageJ application were chosen as methods for determining the chemical and granulometric compositions of the eruption products.

In total, 7 samples were examined, differing in structure, reflection coefficients, colors and dispersion. The images of the samples are shown in Figure 1.

a, b - volcanic ash; c - black rock with a dense fine-grained structure; d - porous rock of black color; e - dense gray rock; f -black rock with brown inclusions; g - red-brown rock

Figure 1 - Test samples

As a result of the conducted research, the following conclusions were made.

1 - according to the histograms of the distribution of ash particles, volcanic ash has an inhomogeneous granulometric composition and refers to coarse-dispersed eruption products with a large spread of e values of particle radii. Ash particles have significantly different linear parameters and area: from 0.674 mm to 13.663 mm, area - from 0.207 mm^2 to 105.513 mm^2. The values of the average effective particle diameters vary from 4.498 mm to 13.242 mm.

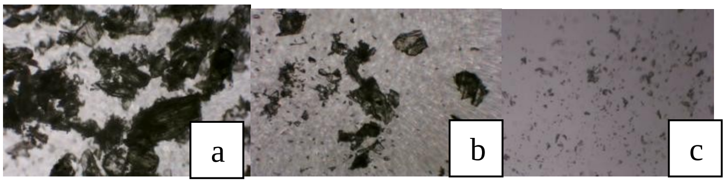

a-particles of the largest size; b-medium size; c-the smallest size

Figure 2 - Micrographs of ash particles of different sizes

2 - the reflection coefficients of the particles are 0.84, 0.48 and 0.46 (Fig. 1, a, b, c).respectively, 1.75 and 1.82 times more than the particles of samples 2 and 3, respectively. The red channel (R) makes the greatest contribution to the image. Since the images have a gray tint, we can say that the values of all channels are approximately equa R:G:B=1:1:1.

3 - The values of the fractal dimensions of ash particles are close to the values of 1.7, which suggests that the resulting curves are wound in space, almost like a surface.

With the help of morphological description and theoretical data, it is possible to make assumptions about t belonging of samples to different rocks: light samples are more rich in silica than dark-colored ones. Object 1 is black in color with a dense fine-grained structure and white inclusions refers to volcanic basalt. Object 2 - an inhomogeneous stony rock of black color of a clastic-porous structure belongs to volcanic tuff. Sample 3, which has a finely porous structure, is a volcanic pumice stone containing a large amount of hematite Fe3O4, which causes its red-brown color. Object 4 is a dense gray bulk with a small content of colored minerals, presumably belongs to dacite. Product 5 characterized by a black color with noticeable large brown inclusions. It characteristically resembles volcanic basalt.

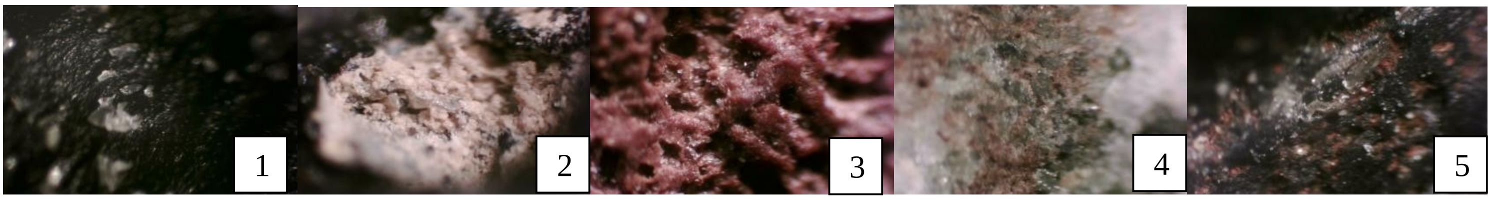

Figure 3 - Micrographs of the studied volcanic rocks

The products of the Nisyros volcano eruption have a diverse chemical composition, both in the first and second order of reflection. The compositions are similar, but differ in the intensity of the characteristic lines. With the help of X-ray fluorescence analysis, it was possible to determine not only the main composition of the studied samples, but also the impurity. The spectrum of iron is characterized by the highest intensity for all objects of analysis.

Table 1 - Basic chemical composition of the products of the Nisyros volcano eruption, Greece

№ sample	1	2	3	4	5	6	7
Basic chemical composition	Mn	Cr	Mn	Mn	Mn	Mn	Fe
	Fe	Mn	Fe	Fe	Fe	Fe	Cu
	Cu	Fe	Cu	Cu	Cu	Cu	Ge
	Zn	Cu	Ge	Rb	Rb	Rb	Sr
	As	Zn	Br	Sr	Sr	Sr	Zr
	Se	As	Sr	Zr	Cd	Tc	Mo
	Br	Br	Y	Tc	Tm	Rh	Tc
	Rb	Rb	Pd	Rh	Re	Pd	Ru
	Sr	Sr	Cd	Pd	Ir	Ag	Rh
	Zr	Zr	Tm	Ag	Bi	In	Pd
	Pd	Pd	Hf	Tm	U	Tm	Ag
	Ag	Ag	Pb	Ir	Np	Re	Cd
	Pd	Pb	Bi	Bi	Pu	Ir	In
	Sn	Sn	Pa	U	Am	Bi	Sn
	Pb	Lu	Am	Np		Po	Ho
	Pu	Hf		Pu		Pu	Hf
	Am	Os					Pb
		Hg					Ac
		Bi					Th
		Po					Pu
		U					
		Th					
		Am					

1 - volcanic ash (1); 2 - dense gray rock; 3 - black rock with brown inclusions; 4 - porous black rock; 5 - brown-red rock; 6 - black rock with dense fine-grained structure; 7 - volcanic ash (2)

Literature

1. Marlina A. Elburg, Ingrid Smet, Elen De Pelsmaeker. Influence of source materials and fractionating assemblage on magmatism along the Aegean Arc, and implications for crustal growth. Geological Society, Londo Special Publications 2014, v. 385; p. 137-150

2. Ben Austin Carret. Geophysical Hazards and Hazard Awareness on Nisiros Volcano, Greece. A dissertation submitted in partial fulfillment of the requirements for the award of MSc in Geophysical Hazards at University College London, 2006

3. J. H. Sterba, G. Steinhauser, M. Bichler. On the geochemistry of the Kyra eruption sequence of Nisyro volcano on Nisyros and Tilos, Greece. Applied Radiations and isotopes, 69. 2011 p. 1605-1612

1B1b

Suppression of spontaneous emission due to intra-atomic interference

Alexander Sadykov

Physics Faculty, Orenburg University, Russia

Spontaneous transitions in the optical and other regions of the electromagnetic spectrum are the main obstacle to the accumulation of energy in the reservoir of excited particles. Spontaneous emission has been shown by Purcell can be suppressed by the surrounding of the emitter. Another possible way to suppress the spontaneous emission is to use the intra-atomic interference in excited particles.

A possibility of the interference suppression of spontaneous transitions may be illustrated by the mechanical model of coupled oscillators that does not need participation of mysterious fluctuations of electromagnetic vacuum.

The quantum evolution of spontaneously emitting particles should be described by the equation for the reduced density matrix:

$$d\hat{\rho}_s^{ex}/dt = -\left\{\left(\sum_i \hat{S}_i^+ \sum_j \hat{S}_j^-\right)\hat{\rho}_s^{ex} + \hat{\rho}_s^{ex}\left(\sum_i \hat{S}_i^+ \sum_j \hat{S}_j^-\right)\right\},$$

where $\hat{S}^+$, $\hat{S}^-$ – are the operators of absorption and emission atomic transitions. The suppression of spontaneous transitions in ensemble of excited particles means that:

$$d\hat{\rho}_s^{ex}/dt = 0 \text{ and } \left(\sum_i \hat{S}_i^+ \sum_j \hat{S}_j^-\right)\hat{\rho}_s^{ex} + \hat{\rho}_s^{ex}\left(\sum_i \hat{S}_i^+ \sum_j \hat{S}_j^-\right) = 0$$

Three models of emitting atomic systems (II-, V-, and Ψ-model) with degenerative excited levels were analyzed.

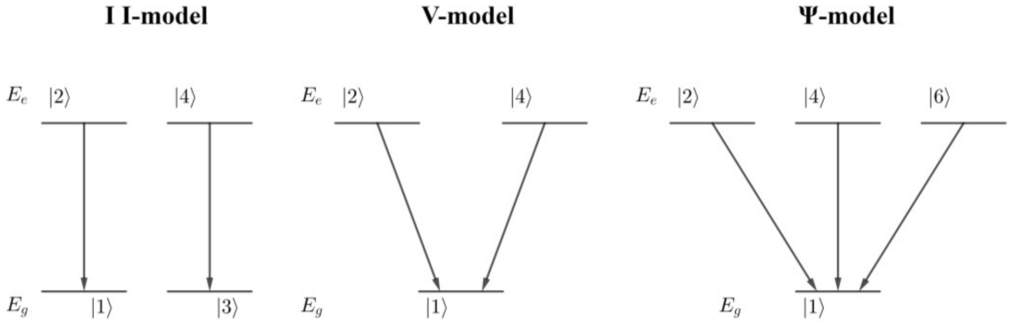

For II-model suppression of spontaneous emission was shown to be impossible. V- and Ψ-models allow the interference suppression of spontaneous transitions as far as they have common ground level. For V-model suppression of spontaneous transitions and radiation will be suppressed if the system will be in the superposition of both excited states

$$|\Phi\rangle = 2^{-1/2}\{|2\rangle - |4\rangle\}.$$

V. L. Ginzburg. The nature of spontaneous radiation. Usp. Fiz. Nauk, 1983, V. 140, p. 687-698,

1B2b

Attempt to synthesize silyl-substituted diphophatetrahedrane: highly strained organophosphorus molecule

Yuta Shimada, Rong Shang, Hiroto Yoshida and Masaaki Nakamoto
Department of Chemistry, Graduate School of Science, Hiroshima University

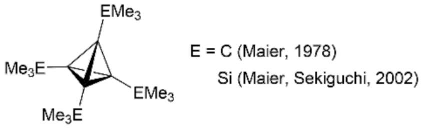

Fig. 1 carbon tetrahedranes

White phosphorus (P_4) is well-known stable tetrahedral molecular, found in 17th century. Hydrocarbon analogues which have the same structure as white phosphorus are called tetrahedranes (C_4R_4) (**Fig. 1**). In 1978, Maier and co-workers reported the first stable tetrahedrane which had bulky ^{t}Bu substituent ($C_4{}^tBu_4$)[1]. In 2002, Maier, Sekiguchi and co-workers succeeded in synthesis of silyl-substituted tetrahedrane ($C_4(SiMe_3)_4$)[2]. Due to the effect of silyl group, the latter tetrahedrane has two characteristic features compared to the ^{t}Bu derivative; increasing thermal stability and ease chemical transformation of functional groups.

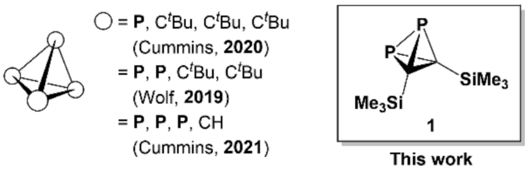

Fig. 2 reported carbon-phosphorus mixed tetrahedranes

Recently, investigation on phosphorus-carbon mixed tetrahedranes; phosphatetrahedranes ($P_n(CR)_{4-n}$; n = 1, 2, 3) have attracted attention because of highly strained reactive P-C σ bonds in the skeleton (**Fig. 2**). In 2019, Wolf and co-workers reported synthesis and isolation of diphosphatetrahedrane ($P_2(C^tBu)_2$)[3]. After that, Cummins and co-workers reported mono- and triphosphatetrahedrane ($P(C^tBu)_3$, P_3CH)[4,5]. These phosphatetrahedranes are expected to be a new building block of novel organophosphorus compounds for its unique reactivity. However, in previous research, only alkyl-substituted phosphatetrahedranes were reported. Thus, we focused on silyl-substituted phosphatetrahedrane. As described in study on silyl-substituted tetrahedrane, bonding and reacting nature affected by silyl group of phosphatetrahedrane is of interest.

In our group, synthesis and property of silyl-substituted tetrahedrane have been investigated. We considered that the method to synthesize the compound was applicable to synthesize phosphatetrahedranes.

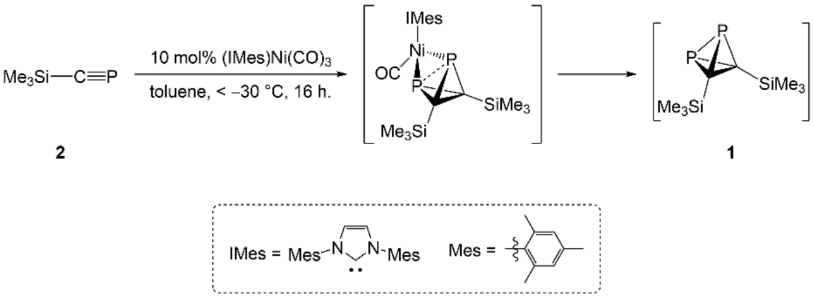

Fig. 3 scheme for synthesis of the target compound

As described in the report of ^{t}Bu-substituted diphophatetrahedrane, formal [2+2] cycloaddition between silyl-substituted phosphaalkyne (**1**, **Fig. 3**) and catalytic nickel(0) complex was carried out (**Fig. 3**). After this reaction, characteristic signal at −394 ppm in $^{31}P\{^1H\}$ NMR spectrum was observed. This remarkably high-field shifted signal indicated generation of highly strained phosphorus compound. In this presentation, attempt to synthesize silyl-substituted diphosphatetrahedrane (**2**, **Fig. 3**) will be reported.

[Ref.] (1) Maier, G.; Pfriem, S.; Schäfer, U.; Matusch, R. *Angew. Chem. Int. Ed. Engl.* **1978**, *17* (7), 520–521. (2) Maier, G.; Neudert, J.; Wolf, O.; Pappusch, D.; Sekiguchi, A.; Tanaka, M.; Matsuo, T. *J. Am. Chem. Soc.* **2002**, *124*, 13819–13826.
(3) Hierlmeier, G.; Coburger, P.; Bodensteiner, M.; Wolf, R. *Angew. Chem. Int. Ed.* **2019**, *58*, 16918–16922. (4) Riu, M.-L. Y.; Jones, R. L.; Transue, W. J.; Müller, P.; Cummins, C. C. *Sci. Adv.* **2020**, *6* , eaaz3168. (5) Riu, M.-L. Y.; Ye, M.; Cummins, C. C. *J. Am. Chem. Soc.* **2021**, *143*, 16354–16357

1B3b

Noncollinear spin and magnetic structures due to hyperfine interactions

Elina Kaepkulova

[1]Department of Physics, Orenburg University, Russia

Chiral organic and nonorganic magnets have many unusual properties. Such noncollinear magnetic structures and magnetic skyrmions are usually thought to be determined by Dzyaloshinskiy-Moria (DM) interaction. However, in real magnetics there are many other interactions that do not commute with the exchange one. One of them is the contact Fermi interaction of electrons with nuclear spins.

$$\widehat{H}_F = (8\pi/3)g_e\mu_B g_n\mu_n \left\{ \widehat{\bar{S}}_1 \widehat{\delta}(\vec{r}_1 - \vec{r}_A) + \widehat{\bar{S}}_2 \widehat{\delta}(\vec{r}_2 - \vec{r}_A) \right\} \widehat{\vec{I}}$$

In spin Hamiltonians this interaction is known as hyperfine interaction (HFI) of the electron spin with nuclear ones. The spin Hamiltonian of exchange and HFI is

$$\hat{H} = J\,\vec{S}_i\vec{S}_j + a_1\vec{S}_1\vec{I} + a_2\vec{S}_2\vec{I} =$$
$$= J\,\vec{S}_i\vec{S}_j + (1/2)(a_1 + a_2)\left(\vec{S}_1 + \vec{S}_2\right)\vec{I} + (1/2)(a_1 - a_2)\left(\vec{S}_1 - \vec{S}_2\right)\vec{I}$$

The antisymmetric part of HFI does not commute with the exchange one. Thus it has been shown to mix election singlet and triplet state and forms noncollinear magnetic structures as well as DM interaction. So the ground state of the electron spin pair will be

$$\left|\Psi\right\rangle = c_S\left|S\right\rangle + c_T\left|T\right\rangle$$

For ground “singlet” state

$$c_S{}^2 = \frac{1}{2}\left(1 + \frac{1}{\sqrt{1+\alpha^2}}\right) \quad c_T{}^2 = \frac{1}{2}\left(1 - \frac{1}{\sqrt{1+\alpha^2}}\right), \qquad \alpha = \frac{(a_1 - a_2)}{J}$$

The angle Θ between electron spins is determined as the quantum average production of spin operators

$$Cos\Theta = \frac{\left\langle\Psi\right|\vec{S}_1 \cdot \vec{S}_2\left|\Psi\right\rangle}{\left|\vec{S}_1\right| \cdot \left|\vec{S}_2\right|}$$

For the distorted singlet state

$$Cos\Theta = -(1 + \frac{2J}{\sqrt{J^2 + (a_1 - a_2)^2}})/3 < -1$$

This inequality means that $\Theta < 180^0$, thus both electron spin deviate from a strictly antiparallel state and form a non-collinear structure as well as in case of DM interaction. The effects can be strong enough if hyperfine constants a_1 and a_2 comparable with the exchange constant J.

1C1b

Conformation of crown ether complexes with alkylammonium ions and its dependence on alkyl chain length under cold gas-phase conditions

Ryosuke Goda,[1] Saya Kanazawa,[1] Shiori Machida,[1] Satoru Muramatsu,[1] Yoshiya Inokuchi,[1]

[1] Department of Advanced Science and Engineering, Hiroshima University

［**Introduction**］ Crown ethers (CEs) show selective inclusion of metal ions and adopt their cavities to effectively encapsulate guest ions.[1] For benzo-CE complexes, UV spectroscopy under cold gas-phase conditions provided information on the conformation. These complexes showed sharp vibronic structures in their UV spectra, allowing the application of UV-UV and IR-UV double-resonance spectroscopy to examine the number of conformers and their structures. For molecular ion guests, primary alkylammonium ions (RNH_3^+) also form stable complexes with CEs. Recently, we studied dibenzo-18-crown-6 (DB18C6) complexes with the RNH_3^+ ions by cold UV spectroscopy in the gas phase [2]. The DB18C6 complexes with RNH_3^+ ions are formed through three N−H···O hydrogen bonds, which induce the formation of a novel encapsulation structure absent in the metal-ion complexes.

In this study, we extend our study to another CE with a different cavity size: benzo-12-crown-4 (B12C4) (Figure 1). We investigated the B12C4 complexes with NH_4^+, $MeNH_3^+$, $EtNH_3^+$, and $PrNH_3^+$ through UV photodissociation (UVPD) and IR-UV spectroscopies performed under cold gas-phase conditions. Subsequently, we carried out quantum chemical calculations to analyze the UV and IR spectra and determine the conformation of the complexes. We elucidated the difference in the conformation of the B12C4 complexes between the ammonium and K^+ guests and the origin of the difference at the molecular level [3].

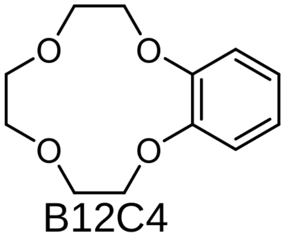

Fig. 1 Structure of B12C4

［**Experimental**］ The experiment was performed with our spectrometer under cold gas-phase conditions.[3] B12C4 complexes with NH_4^+, $MeNH_3^+$, $EtNH_3^+$, and $PrNH_3^+$ were produced by electrospraying methanol solutions of B12C4 and RNH_3Cl salt. These complexes were introduced into a cold, Paul-type quadrupole ion trap (QIT). The QIT was cooled to ~4 K using a He cryostat, and the He buffer gas was continuously introduced into the QIT. These ions were stored in the QIT for ~90 ms and then cooled translationally and internally by collision with cold He buffer gas. The UVPD spectra were obtained by plotting the yields of fragment ions against the wavenumber of the UV laser. In the IR-UV double-resonance experiments, the wavenumber of the UV laser was fixed and the intensity of the fragment ions was monitored. The output of an IR laser (LaserVision) was introduced to the QIT 100 ns before the UV laser while scanning the wavenumber of the IR laser in the CH and NH stretching (2700−3500 cm^{-1}) region. The IR-UV dip spectra were obtained by plotting the ratio of the fragment ion intensity with the IR laser on/off (I_{on}/I_{off}) as a function of the wavenumber of the IR laser. Quantum chemical calculations were performed with the GAUSSIAN16 program package at the ωB97X-D/6-311++G(d,p) level of theory to obtain stable structures of the complexes and assign the UVPD and IR-UV spectra.

［Results and Discussion］ Figure 2 displays the UVPD spectra of the NH_4^+(B12C4), $MeNH_3^+$(B12C4), $EtNH_3^+$(B12C4), and $PrNH_3^+$(B12C4) complexes (red curves). For reference, the UVPD spectrum of the K^+(B12C4) complex is shown in Figure 1a. All of the ammonium ion complexes exhibited sharp 0-0 bands around 36480 cm^{-1}. Remarkably, the UVPD spectra of the $EtNH_3^+$(B12C4) and $PrNH_3^+$(B12C4) complexes exhibited new vibronic progressions other than those of the 0-0 band (i.e., around 36700 cm^{-1}). The interval of the progressions was ~34 cm^{-1}, as shown by the solid black lines in Figure 1d,e.

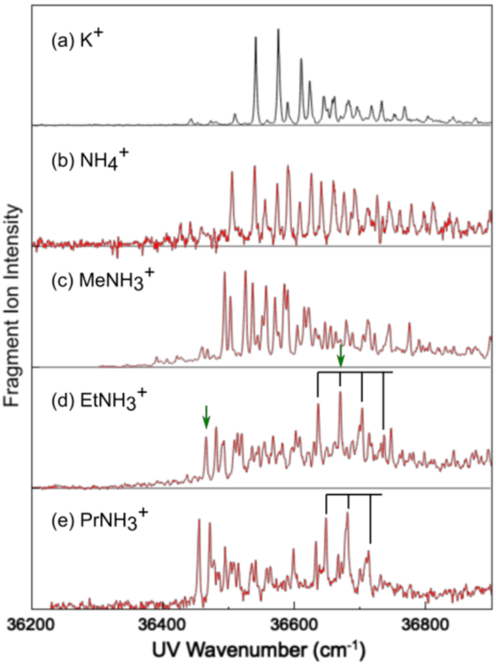

Fig. 2 UVPD spectra of RNH_3^+(B12C4) complexes

For the $EtNH_3^+$(B12C4) complex, two distinct IR spectra were observed to be dependent on the UV probe wavelength indicated by arrows in Figure 2. The IR-UV spectra are shown in Figure 3. A sharp band was observed in the IR-UV spectra at 3348 and 3345 cm^{-1}. These bands can be assigned to free NH stretching vibrations. The IR-UV results indicate that at least two conformers exist in the $EtNH_3^+$(B12C4) complex.

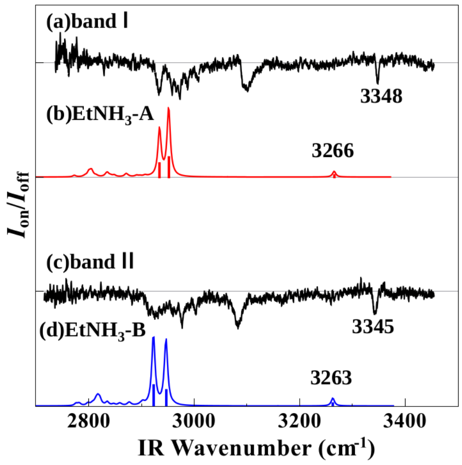

Fig. 3 IR-UV dip spectra and calculated IR spectra of $EtNH_3^+$(B12C4)

Figure 4 shows the side view of a couple of isomers (Et-a and Et-b) of the $EtNH_3^+$(B12C4) complex. In the isomer Et-a, the benzene moiety and crown ring are oriented almost perpendicular to each other. As the NH_3^+ group of the $EtNH_3^+$ guest is bound to the crown ring through the N−H···O hydrogen bonds, the $CH\cdots C_{benzene}$ distance between the ethyl group and the benzene ring becomes long (3.87 Å; Figure 4). In Et-b, the benzene ring and crown cavity were situated almost on the same plane. As a result, the CH bond of the ethyl chain and the benzene ring can become close to each other (2.77 and 3.00 Å in isomer EtNH3-b), providing C−H···π interactions, and stabilizing isomer Et-b.

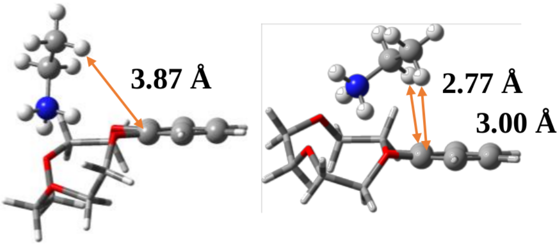

Et - a (1.3)   Et - b (0)

Fig. 4 Stable structures of $EtNH_3^+$(B12C4) and total energy (kJ mol^{-1}) relative to most stable structure

［Reference］

[1] Pedersen, Science. 241, 536 (1988). [2] Kubo *et al.*, *J. Phys. Chem. A*, 124, 3228 (2020). [3] Goda *et al.*, *J. Phys. Chem. A*, in press.

1C2b

Production and study of the stability of suspensions of paraffin wax modified with polyethylene glycol

Diyanova Yulia,[1] Yudin Alexander[1], Salnikova Elena[1]

[1]Department of Chemistry, Faculty of Chemistry and Biology, Orenburg State University

The purpose of this work is to select the conditions for obtaining a stable suspension of highly purified paraffin grade P-2.

There are a number of techniques for preparing suspensions, which are mainly based on dispersing molten paraffin in water. Dispersion can be carried out using vigorous stirring, ultrasound, high pressure, and so on. With a decrease in temperature during dispersion, the dispersed phase - paraffin - solidifies. To stabilize paraffin particles, surfactants (surfactants), silicon dioxide nanoparticles can be used.

In this study, a nonionic surfactant, polyethylene glycol (PEG), was used as a stabilizer for paraffin suspensions. The choice of this surfactant is primarily due to its high rate of biodegradability in wastewater, chemical resistance in hard water, and human safety.

At the first stage of research, to obtain suspensions, dispersion was used with the use of intensive stirring (one thousand revolutions per minute) with heating the mixture of components to 80 degrees.

For the obtained suspensions, the concentration of suspended substances was determined by nephelometry, the particle size was determined by optical microscopy. The results are shown in Table 1.

Table 1 - Parameters of paraffin particles obtained by the method of intensive mixing

Mixture	Composition	Particle size, μm	Concentration, mass. %
Mixture 1	5% P-2, 95% H_2O	-	-
Mixture 2	5% P-2, 5% PEG, 90% H_2O	185,345 ± 17,660	0,3 %

Based on the results obtained, it can be seen that, in the absence of polyethylene glycol, the formation of a stable suspension does not occur; when PEG is added in an amount of five percent of the mass, a suspension is formed with an average particle size of one hundred and eighty five micrometers. However, the concentration of the suspension is very low, the resulting suspension does not make sense to use for ion flotation and sorption processes.

To increase the concentration of the water-paraffin suspension and reduce the size of dispersed particles, it was decided to use the method of ultrasonic dispersion. The results are shown in Table 2.

Table 2 - Parameters of paraffin particles obtained by the method of ultrasonic dispersion

Mixture	Composition	Particle size, μm	Concentration, mass. %
Mixture 1	5% P-2, 95% H_2O	87,446 ± 25,496	1,22 %
Mixture 2	5% P-2, 5% PEG,	62,882 ± 5,496	7,32 %

	90% H_2O		

Based on the data obtained, it can be concluded that the use of ultrasonic dispersion leads to the production of water-paraffin suspensions with high concentrations and a small particle size, of the order of sixty two micrometers. The resulting suspensions are highly stable and remain stable for two or more weeks. The introduction of polyethylene glycol leads to an increase in the concentration of dispersed particles seven times compared with the mixture number 1.

On figure 1 shows a micrograph of paraffin particles obtained by ultrasound in the presence of PEG.

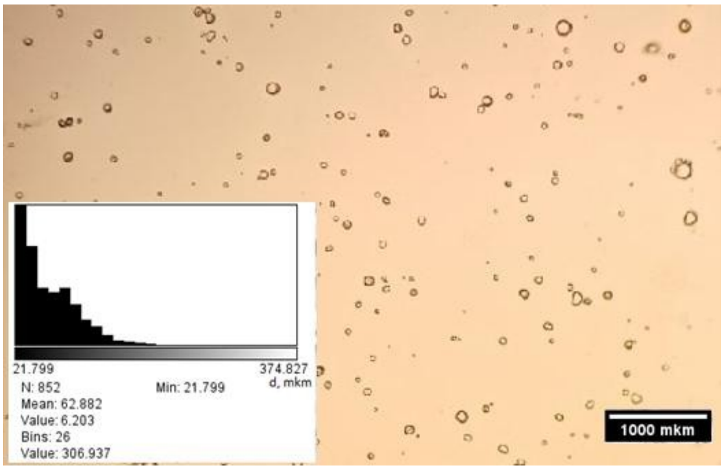

Figure 1 - Dispersed paraffin particles obtained by ultrasonic dispersion in the presence of 5% of the mass. polyethylene glycol

To assess the sorbing properties, a suspension of paraffin with PEG obtained by ultrasonic dispersion was mixed with a model solution containing cerium ions, after which the solid particles were separated by filtration through a membrane made of cellulose acetate with a pore size of zero point two micrometers, then washed three times on a filter with distilled water, dried under vacuum, and the residual cerium content in the resulting material was estimated by X-ray fluorescence analysis.

According to the results of spectral analysis, it can be seen that the sample under study contains a significant amount of cerium ions; therefore, paraffin suspensions with various modifiers can be used as promising materials for extracting valuable elements from poor ores and industrial waste by sorption, solid-phase extraction, and ion flotation.

List of sources used:

1 Novopoltseva, T.S. Span 80 and Tween 80 Stabilized Paraffin and Stearic Acid Solids / T.S. Novopoltseva [et al.] // Advances in chemistry and chemical technology. 2017. No. 13 (194). S. 40-41.

2 Cho, K. Experimental study on the application of paraffin slurry to high density electronic package cooling / K. Cho, M. Choi // Heat and Mass Transfer. – 2000. – Vol. 36. – No 1. – P. 0029-0036.

3 Zelepukin I.V., Shipunova V.O., Mirkasymov A.B., Nikitin P.I., Nikitin M.P., Deyev S.M. Synthesis and Characterization of hybrid core-shell Fe3O4/SiO2 nanoparticles for biomedical applications // Acta Naturae (English version). 2017. №4 (34).

1C3b

Inactivation of bacteria in solutions by shock acoustic waves

Dorofeev D.V., Doroshkevich A.V., Tsurko D.E.

Russia, Orenburg, Orenburg University

The ability of pathogenic bacteria to develop resistance to antibiotics initiates the search for new ways of inactivation, to which they will not be able to develop immunity. At the same time, methods of defeating pathogens that act efficiently and quickly are required [1-2]. Photodynamic treatment with the participation of reactive oxygen species (ROS) satisfies such requirements of exposure to living microorganisms [3-6]. However, photodynamic action is effective only in highly aerated transparent media in which exciting light penetrates deep layers. Shock waves can be used to affect microorganisms in deep layers of opaque media. If the shock wave is excited by rapid local heating of the medium for a time of ~ 1 ns, then the length of the wave front will be ~ 1.5 microns, which is commensurate with the size of bacteria ~ (1-5) microns and with sufficient amplitude will be detrimental to microorganisms. It is convenient to produce rapid local heating of the medium using thermosensitizers (TS) irradiated with short pulses of laser radiation [7]. At an excitation power density exceeding 5-8 MW/cm ^{2}, TS molecules are capable of absorbing two (or more) incident radiation quanta and stepwise passing through real lower singlet S_1 or triplet T_1 levels into high electron-excited states (HEES) [8-9]. Nonradiative relaxation In the IVS of molecules provides rapid local heating of the medium, which generates shock waves. The objects of the study were strains of *Salmonella Typhimurium* LT2 and *Staphylococcus Aureus*. Model dyes erythrosine (anion) and rhodamine C (cation) were used as TS. To photoinactivate bacteria, suspensions with dyes in a cuvette were excited by pulses of focused laser (YAG:Nd laser LQ-215) radiation ($\lambda = 532$ nm, $P \geq 8$MW/cm^2). Dye-cations bind to the outer wall of *S.typhimurium* bacteria due to electrostatic interaction. Neutralization of the charge of the outer wall of the cells leads to the fact that the bacteria "stick together" into large aggregates, about 5-10 microns in size. Such aggregates are very effectively destroyed by shock waves. Unlike salmonella, *S.aureus* bacteria already exist in their natural state mainly in the form of clusters, about 10 microns in size. Such clusters are also effectively destroyed by shock waves. Shock waves also damage individual bacteria. In order to identify the nature of damage to individual bacteria, ROS images and UV absorption spectra of solutions before and after irradiation were analyzed. The appearance of absorption maxima at wavelengths of 260 nm and 280 nm after irradiation indicates the destruction of the walls of individual bacteria. With low-intensity exposure to photosensitizers (PS) by laser radiation, the main agents acting on pathogenic microorganisms are ROS. Switching to the excitation of sensitizers by nanosecond pulses of high-power density light leads to a "switching" of the mechanism of action on bacteria. Despite the fact that the concentration of ROS increases, the probability of energy transfer from PS molecules to the environment increases, and conditions for local hyperthermia are created, the destruction of cells by shock waves becomes the main mechanism of bacterial damage. The waves not only destroy the natural formations of bacteria (clusters of staphylococci) and conglomerates that occur when bacteria "stick together" while neutralizing the charge of the outer wall, but also destroy the walls of individual cells with high efficiency. Shock waves can inactivate cells at a great distance from the excitation zone. This mechanism of destruction of bacteria in solutions is very effective in case of insufficient penetration of light or oxygen into the medium. The results obtained can be useful in the development of new antibacterial methods.

1. J. O'Neill Tackling a global health crisis: initial steps. The Review on Antimicrobial Resistance Chaired by Jim O'Neill, 2015.
2. Taylor P.W., Stapleton P.D., Luzio J.//Drug Discov. Today. 2002. V. 7. P. 1086. https://doi.org/10.1016/s1359-6446(02)02498-4
3. Kashef N., Huang Y., Hamblin M.R.// Nanophotonics. 2017. V. 6(5). P. 853. https://doi.org/10.1515/nanoph-2016-0189.
4. Kim, M.-J. // Food Control. 2017. №82. P. 205-315. https://doi:10.1016/j.foodcont.2017.06.040.
5. Adriele, R.S. // Antibiotics. 2019. 8(4). P. 1-13. https://doi:10.3390/antibiotics8040211.
6. Letuta S.N., Pashkevich S.N., Ishemgulov A.T. et al. // J. Photochem. Photobiol. B. 2016. V. 163. P. 232. https://doi.org/10.1016/j.jphotobiol.2016.08.036.
7. Cleary S.F., Laser Applications in Medicine and Biology, Plenum Press, New York, 1977, P. 175-219.
8. Orner G.C., Topp M.R. // Chem. Phys. Lett., 1975, v. 36, № 5, p. 295-300.
9. Nagaoka C., Fujita M., Takemura T., Baba H. // Chem. Phys. Lett., 1986, v. 123, № 6, p. 489-492.

2A1a

Cs desorption from clays and clay minerals by quaternary ammonium cations: the role of ammonium head group structures

Herry Wijayanto,[1,2] Satoru Nakashima[1,2,3]
[1] Radioactivity Environmental Protection Course, Phoenix Leader Education Program, Hiroshima University
[2] Department of Chemistry, Graduate School of Science, Hiroshima University
[3] Natural Science Center for Basic Research and Development (N-BARD), Hiroshima University

Quaternary ammonium cations (QACs), commonly known as cationic surfactants, are positively charged compounds with NR_4^+ structure where N is nitrogen atom, and R is alkyl chain consisting of C and H atoms. Recently, the study of single-long-chain QACs as Cs desorption agents continues to be concerned in response to the soil decontamination after Nuclear Power Plant accident in Fukushima.[1,2,3] Moreover, alkyl chain lengths of QACs strongly contributed to the Cs desorption from clay minerals. The longer the alkyl chain, the more Cs were released from kaolinite due to the stronger affinity of longer chain length with kaolinite surfaces.[4] In the case of montmorillonite, a longer alkyl chain increased its interlayer distance, therefore enhancing Cs desorption efficiency.[2] Although the influence of QACs alkyl chain has been investigated well, the role of ammonium head group type of QACs toward Cs desorption had not much been highlighted. This study examined the use of benzyldimethyldodecylammonium bromide (BDAB) and dodecyltrimetylammonium bromide (DTAB) (Fig. 1) having similar alkyl chain lengths but different head group types to desorb Cs from the sample of clays (Na- and Ca-bentonite) and clay minerals (kaolinite and illite).

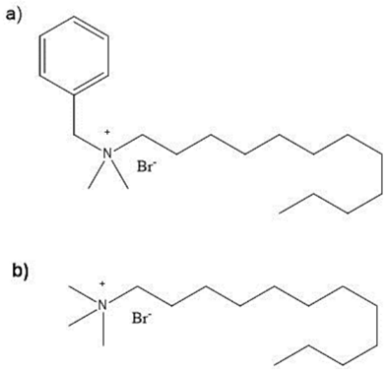

Fig. 1. Structure of (a) BDAB and (b) DTAB

Samples were first contaminated by Cs solution with maximum adsorption capacity, followed by desorption experiment using desorbents. Batch desorption experiment indicated that, in general, desorption efficiency for all studied samples increased by increasing QACs concentration. In swelling bentonites that highly contain montmorillonite, Cs desorption was accompanied by interlayers' expansion. In the case of Na-bentonite, BDAB showed higher Cs desorption efficiency than DTAB due to larger Na-bentonite interlayers expansion after intercalation of BDAB (bulkier ammonium head structure). In contrast, Cs desorption efficiency from Ca-bentonite was relatively similar, which corresponded to the identical interlayers' expansion after intercalation of both QACs. It was because divalent cation of Ca^{2+} must associate with negative charge of interlayer, limiting interlayer expansion of Ca-bentonite.

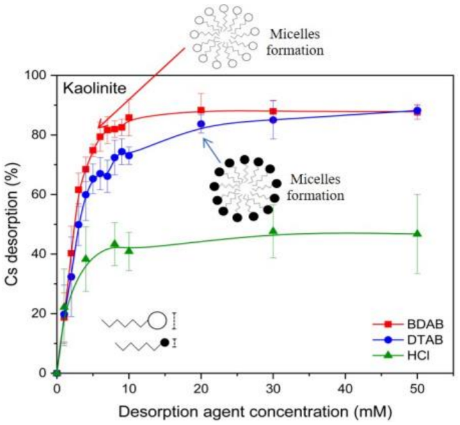

Fig. 2. Cs desorption from kaolinite

Cs desorption from kaolinite was more governed by surfactant micelles. In comparison to surfactant ions, surfactant micelles had a stronger affinity to the clay surface, enhancing Cs desorption efficiency. Fig. 2. shows that as the surfactant micelle formed earlier for BDAB, a faster Cs desorption was achieved. Thus, BDAB desorbed Cs efficiently than DTAB due to formation of surfactant micelle at low concentration in BDAB solution.

For Cs desorption from illite, both QACs even showed relatively similar performance with HCl used as a desorbent control. This was due to the existence of frayed edge sites in illite, which provokes strong cesium retention. Desorption kinetic model of pseudo-second order fitted well to all studied samples by BDAB and DTAB suggested that desorption process was ion-exchange process.

References

1) C. W. Park, B. H. Kim, M. Yang, B. K. Seo, J. K. Moon, and K. W. Lee, Chemosphere **168**, 1068-1074 (2017).
2) B. H. Kim, C. W. Park, H. M. Yang, B. K. Seo, S. J. Park, and K. W. Lee, JNFCWT **15**, 1, 27-34 (2017).
3) H. Wijayanto, M. Tsujimoto, T. Basuki, and S. Nakashima, AIP-CP, 2381, 020107 (2021).
4) C. Willms, Z. Li, L. Allen, and C. V. Evans, Appl. Clay Sci. **25**, 125-133 (2003).

2A2b

Flame synthesis of carbon nanoparticles and study of their properties.

Artem Stepanov, Polina Ponomareva
Department of Chemistry, Faculty of Chemistry and Biology,
Orenburg University, Russia

Technical carbon (soot) is a highly dispersed product of incomplete combustion or partial decomposition of hydrocarbons contained in natural and industrial gases, as well as in petroleum and coal oils. Mainly composed of carbon (at least 90%); contains 0.3 nitrogen; up to 10% chemisorbed Oxygen; 0.5% mineral impurities.

Commercial processes to produce carbon black are based on the decomposition of hydrocarbons under the influence of high temperatures. The formation of soot in some cases occurs in a flame of raw materials burning with a lack of air, in others - during thermal decomposition of raw materials in the absence of air. Some types of soot are obtained by extracting it from the synthesis products (and in some cases from decomposition) of various hydrocarbons (for example, in the synthesis of acetylene from methane). Each of these methods for producing soot has several varieties.

When receiving soot in the current of the flame of a paraffin candle on the electrodes, we can get nano globular particles.

Nano globular particles are nano-sized carbon, which is formed in the form of soot when carbon is burned and when using other methods of its production. It has an amorphous appearance and properties that are different from other modifications of carbon.

In the modern world, nano globular carbon is produced on an industrial scale (carbon black, soot) as fillers in rubbers and other polymeric materials. In addition, on its basis, unique composite materials have been developed, which have found application as adsorbents and catalyst carriers. A promising area of using nanostructured carbon materials is the storage of chemical and electrical energy (chemical current sources, supercapacitors, fuel cells, containers of hydrogen and methane).

When organic substances are burned, especially if they have strong smoky properties, particles of very small sizes, including fractal ones, can be formed. However, there are quite a few of them, which does not allow the use of a simple separation of them from the flame. In this work, the method of using a nickel electrode in the form of an iron-nickel alloy, platinide, was considered. To create the flame, hand-made paraffin candles of different compositions were used. A qualitative sign of the production of nano globular particles is the release of an amorphous mass at the minus electrode, which serves as an anode in this process.

When a candle burns, evaporating paraffin vapors burn out in the main part, during the combustion process, carbon decomposes, ionizes and oxidizes. With the introduction of electrodes into the system, it is possible to deionize the gas, which will make it possible to obtain nanoglobular amorphous particles of a spherical shape.The composition of the candles can be seen in Table 1.

Table 1 - Composition of candles

Candle number	Mass, g	Paraffin, %	Polyethylene,%
1	19,1233	100	0
2	19,1335	95	5
3	19,1279	98,75	1,25

Electrodes were introduced into the flame of a candle with electrodes connected to the network using direct current. DC current was obtained using a laboratory power supply, with a voltage of 30 V.

With a decrease in voltage, the intensity of particle production decreases, and more time is required for the accumulation of material.

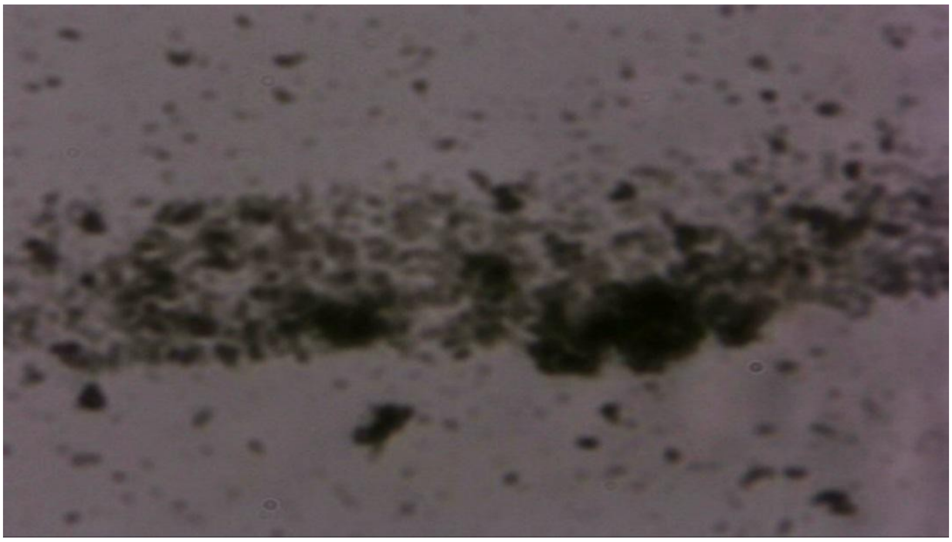

Figure 1 - Image of particles by immersion microscopy

Then the particles were used for the sorption of iron ions from a standard solution of iron-ammonium alum with an iron ion concentration of 0.02 n, followed by drying and washing the particles. After that, nano globular carbon was sent for high-quality X-ray fluorescence analysis in order to reveal the presence of iron ions(figure 2).

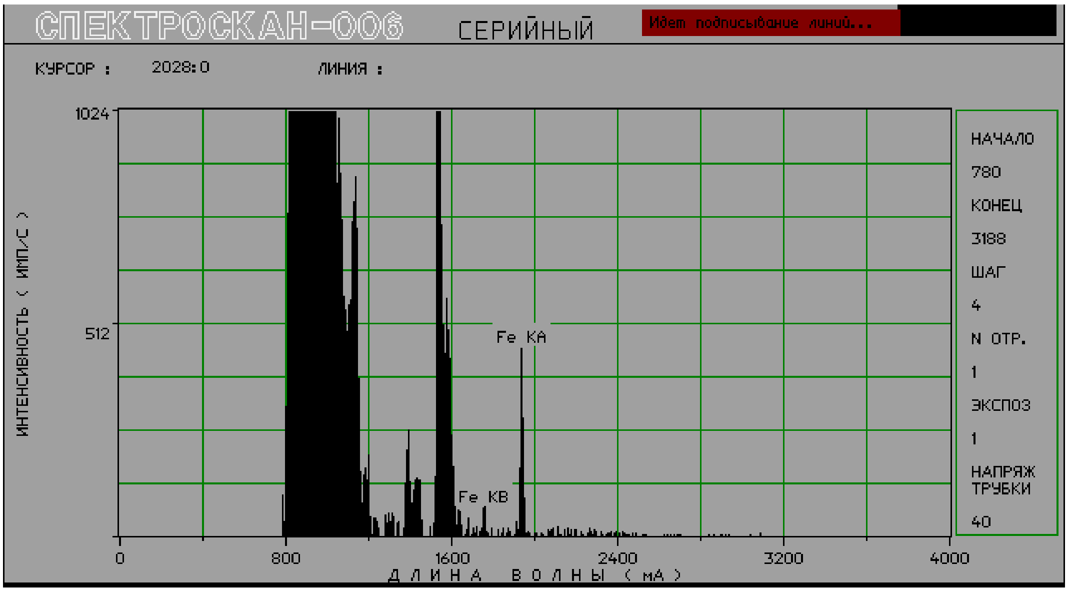

СПЕКТРОСКАН-006 СЕРИЙНЫЙ

Идет подписывание линий...

КУРСОР : 2028:0

ЛИНИЯ :

НАЧАЛО 780

КОНЕЦ 3188

ШАГ 4

N ОТР. 1

ЭКСПОЗ 1

НАПРЯЖ ТРУБКИ 40

Figure 2 - X-ray fluorescence spectrogram

From the obtained characteristic peaks, one can see that the lines of iron are expressed quite well, which makes it possible to judge the presence of iron in the sample, thereby confirming the sorption characteristics of nano globular carbon particles.

Nano globular particles obtained by the flame method have sorption capacity. In further studies, it is planned to consider quantitatively the adsorption characteristics. It is planned to consider the relationship between the shape of nanoparticles and the frequency of the current, including changing the voltage at the electrodes and forming both direct current and alternating current.

List of sources used:

1) Marnautov N.A., Komissarova L.Kh., Tatikolov A.S., Larkina E.A., Elfimov A.B., Vasilkov O.O. development of an optimal method for obtaining homogeneous chemical composition and size magnetite nanoparticles for biomedical purposes // Advances in modern natural science. - 2017. - No. 6. - P. 23-27; URL: https://natural-sciences.ru/ru/article/view?id=36493 (date accessed: 11/28/2021).

2) Preparation of composites with globular carbon nanoparticles distributed in an amorp hous carbon matrix / I. V. Anikeeva, V. S. Solodovnichenko, Y. G. Kryazhev, V. A. Drozdov // Solid Fuel Chemistry. – 2012. – Vol. 46. – No 4. – P. 271-274. – DOI 10.3103/S0361521912040039.

2A3b

Development of cryogenic gas-phase spectrometer aiming for mechanistic study of metal cluster catalysts

Yasuaki Hirokawa,[1] Akihito Matsuyama,[1] Jidai Iriguchi,[1] Yuki Nakahigashi,[1] Masahiro Koyama,[2] Satoru Muramatsu,[1] Yoshiya Inokuchi,[1]

[1] Department of Chemistry, Graduate School of Advanced Science and Engineering, Hiroshima University

[2] Department of Chemistry, School of Science, Hiroshima University

Introduction

Metal clusters, composed of several to hundreds of metal atoms, have unique electronic and geometric structures different from the bulk counterparts, resulting in functions such as catalytic activity. In particular, recent studies have succeeded in application of ligand-protected metal clusters (Fig. 1) for oxidation catalysis.[1] How can the oxygen molecule adsorb on metal surface apparently blocked by the ligands, and how is it activated (Fig. 1)? High-resolution spectroscopy under cryogenic gas-phase condition will allow access to such detailed structural information. However, typical spectrometers now used are optimized for only small molecules with molecular weights of ~500 Da, so that novel apparatus is required for spectroscopic study of the metal clusters of as large as ~10000 Da. In this talk, we report our current status on developing the new spectrometer.

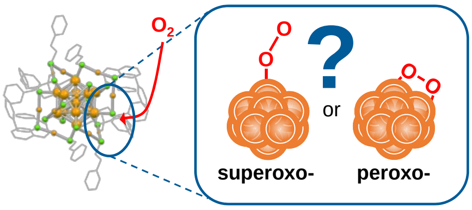

Fig. 1. Ligand-protected metal cluster and predicted adsorption structures.

Results and discussion

Fig. 2 shows a schematic image of the apparatus under development, composed of electrospray ionization (ESI) source, octupole ion guide (OPIG), cryogenic quadrupole ion trap (QIT; ~4 K), and time-of-flight mass spectrometer (TOF-MS). The ions in the QIT are irradiated with laser output to undergo photodissociation, where the fragment ions are detected by TOF-MS. Fig. 3a shows thus obtained ultraviolet photodissociation (UVPD) spectrum of a test sample (K^+·B18C6), recorded by plotting the ion intensity of fragment ion (K^+) against the wavelength. It exhibits well-resolved vibronic bands due to the successful cryogenic cooling, which well reproduces the previous report.[2] In the presentation, details of the apparatus and interpretation of the spectrum are discussed.

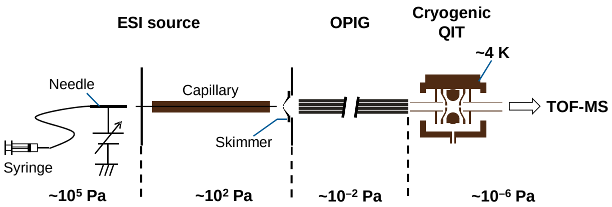

Fig. 2. Photodissociation spectrometer for cryogenic ions under development.

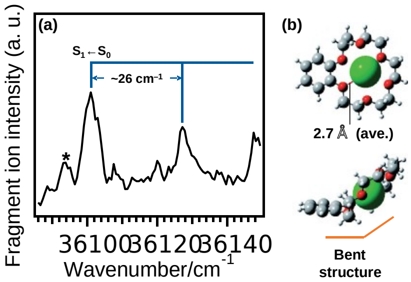

Fig. 3. (a) The UVPD spectrum of K^+•B18C6 measured by the apparatus under development. The peak indicated by an asterisk is attributed to a hot band. (b) Structure of the K^+•B18C6 complex optimized at the M05-2X/6-31+G(d) level.[2]

[1] Nie, X. et al., *ACS Nano* **2012**, *6*, 6014.

[2] Inokuchi, Y. et al., *J. Phys. Chem. A* **2012**, *116*, 4057.

2B1b Mechanism and nonlinear heating kinetics of titan oxide by microwaves

Saniya Sokabaeva
Department of Biophysics and Condensed Matter Physics, Orenburg University, Russia

In the materials manufacturing sector, energy efficiency, sustainability, and economic viability have become increasingly important to industry and society in recent years. Microwave (MW) methods can help to achieve these criteria by providing rapid processing, increased energy efficiency, and reduced equipment costs. MW methods not only offer potential solutions to industry but also provide the added attraction to materials chemists of the opportunity to access new and potentially metastable materials and understand the interaction of solids with electromagnetic fields. For many years, MW heating techniques have been known to offer faster, simpler, and more cost-effective processes, often affording high-yield, high-purity products.1 MW synthesis.

Nonlinear effects were often observed during microwave processing of ceramic oxides, this figure shows the difference in the heating kinetics of stoichiometric TiO_2 and non-stoichiometric titanium oxide $Ti_{2-x}O_2$. Heating of TiO_2 occurs linearly and quickly to a temperature of 800 ^{0}C, stoichiometric heats up in the same microwave field, heats up slowly non-linearly, the purpose of my work is to explain the nonlinear heating of titanium oxide in a microwave field.

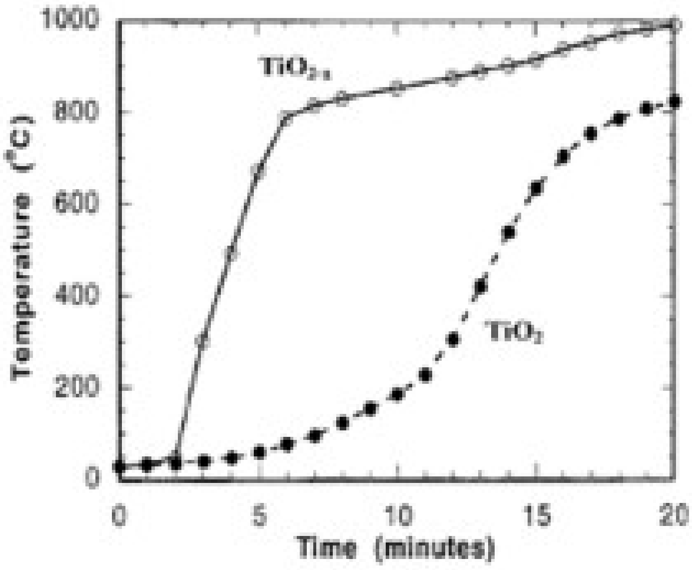

Figure 1. MW absorption characteristics of regular TiO_2 (in air) and reduced $Ti_{2-x}O_2$ (in N_2 atmosphere).

Mathematical model of microwave heating of semiconductive TiO_2 introduce. Nonlinear kinetics of the semiconductive TiO_2 is due to microwave activation of bonded and free electrons. Microwave heating of stoichiometric semiconductive TiO_2 occurs due to Joule heating by conduction electrons rather than electric dipole absorption.

Kitchen, H. J.; Vallance, S. R.; Kennedy, J. L.; Tapia-Ruiz, N.; Carassiti, L.; Harrison, A.; Whittaker, A. G.; Drysdale, T. D.; Kingman, S. W.; Gregory, D. H. Modern Microwave Methods in Solid-State Inorganic Materials Chemistry: From Fundamentals to Manufacturing. Chem. Rev. 2014, 114, 1170–1206, DOI: 10.1021/cr4002353

2B2b

Development of metal nanoparticles doped on lipophilic nanographene

Shusaku Takahahsi, Ryo Sekiya, Takeharu Haino
Department of Department of Chemistry, Graduate School of Advanced Science and Engineering , Hiroshima University

Nanographenes, also known as graphene quantum dots, have received a great deal of attention. Nanographenes prepared by oxidative cleavage have the vast π-conjugating plane. This surface is utilized for doping metal nanoparticles. Although there are limited examples of nanographene which is not soluble in organic solvents, we have been developing functionalized nanographenes that are soluble in organic solvents by introducing organic substituents at the edge of nanographene. In this study, we aimed to create metal nanoparticles doped lipophilic nanographene.

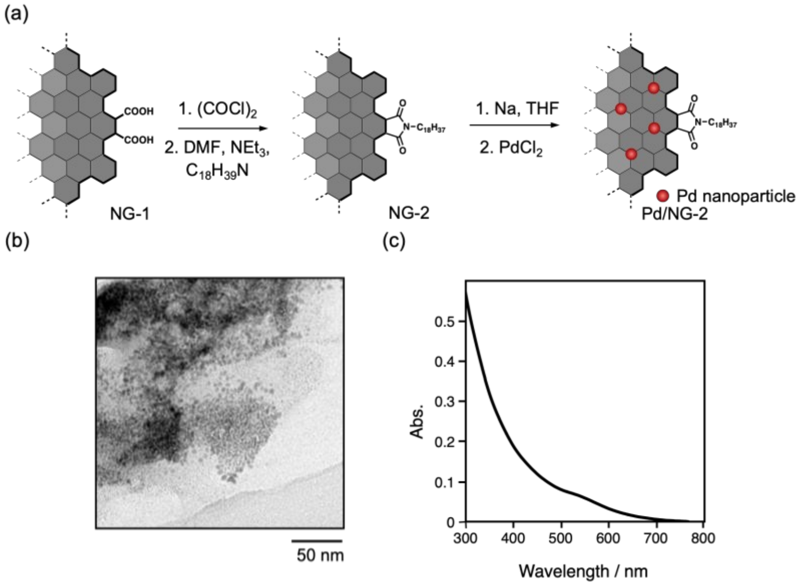

Fig.1.(a)Synthesis of Pd/NG-2 (b)TEM image of Pd/NG-2(C)UV spectrum of Au/NG-2

Edge-functionalized nanographenes(NG-2) were obtained by introducing organic substituents at the edge of nanographene. We achieved the formation of Pd doped nanographene(Pd/NG-2) after reducing the lipophilic nanographene with sodium and adding metal salts such as palladium chloride. TEM and Energy dispersed X-ray spectroscopy(EDS) measurements showed the formation of Pd nanoparticles on the NG-2. (Fig.1b) The formation of different nanoparticles was also achieved as same method and we confirmed the formation of Pd, Au, Ag, Cu, Fe, Pt, Ni nanoparticles. In the case of Au, Ag, a weak band assignable to localized surface plasmonic resonance were detected which supports the formation of nanoparticles. We are now investigating applications for catalysis.

2B3b

Definition of the chemical activity of silicon oxide nanoparticles

Biksenteev Albert,[1] Yudin Alexander[1]

[1]Department of Chemistry, Faculty of Chemistry and Biology, Orenburg State University

In the modern world, interest in nanoparticles is constantly increasing, which is due to the desire for miniaturization of products and the development of new technological methods that are based on the principles of self-assembly and self-organization. Nanoparticles are increasingly being used in various fields of fundamental and applied science, and their use in industry is growing: in the field of high-precision technologies, in ceramics and metallurgy, in nano- and micron coatings.

The aim of this work was to determine the chemical activity of silicon dioxide nanoparticles in comparison with micron powder.

The peculiarity of the nature of solid nanoparticles of silicon dioxide predetermines its chemical properties - the ability to enter into polymer-analogous reactions, that is, reactions affecting functional groups and radicals on the surface of a solid.

The simplest reaction demonstrating the chemical activity of silicon dioxide nanoparticles is the interaction with water and the formation of polysilicic acids, which are capable of complexation reactions with the participation of surface ligands. In the ≡Si – OH group, a silicon atom can form a coordination bond by the donor-acceptor mechanism with water molecules:

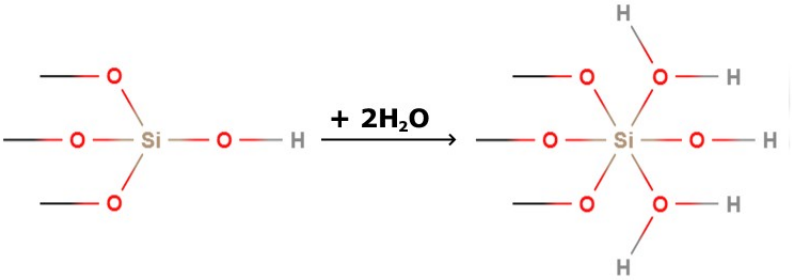

In this case, the coordination number of silicon increases from four to six.

For the experimental determination of the chemical activity, nanosized particles of silicon dioxide obtained by the spray pyrolysis method (sample 1) and micron particles obtained by the sol-gel method with subsequent drying and dehydration (sample 2) were taken. The average particle diameter of sample № 1 was 89 nm, sample № 2 - 270 μm (figure 1).

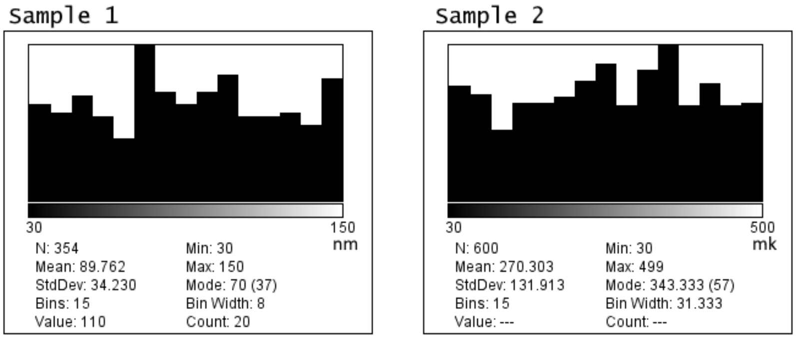

Figure 1 - Distribution of particle diameters of the test samples

The chemical activity of the samples under study was determined by the quantitative content of silicic acid in an aqueous suspension by a photometric method with ammonium molybdate. The results of determining the activity are presented in table 1.

Table 1 - Determination of the chemical activity of silicon dioxide

Sample	Sample weight, g	A	Active SiO_2 mass, mg (according to the graph)	Activity, %
1	0,2088	0,078	0,05268	24,52 ± 0,74
	0,2052	0,074	0,05012	
	0,2042	0,072	0,04885	
2	0,2011	0,005	0,0059	3,01 ± 0,21
	0,2049	0,006	0,0066	
	0,2042	0,005	0,0059	

The experimental results show that nanosized silicon oxide has significant chemical activity, while micron powders exhibit insignificant chemical interaction with water. Almost a quarter of the studied sample of silicon dioxide nanoparticles, due to the large specific surface area, is able to actively enter into chemical interaction and behave like a silicate ion. In general, with the transition from micro-dimension to nano-dimension, the chemical activity increases almost eightfold.

Thus, it has been shown that nanoparticles of a substance inert with respect to water (SiO_2) in a micro size have a sufficiently high affinity for interaction with a decrease in size by three orders of magnitude.

List of sources used:

1 Vert, M .; Doi, Y .; Hellwich, KH; Hess, M .; Hodge, P .; Kubisa, P .; Rinaudo, M .; Schué, FO (2012). "Terminology for biorelated polymers and applications (2012 IUPAC Recommendations)". Pure and Applied Chemistry. 84 (2): 377 p.

2 ISO / TS 80004-2: Vocabulary for nanotechnology Part 2: Nano-objects. International Organization for Standardization. 2015. Retrieved January 18, 2018.

3 Kambalina, MG Determination of the total concentration and forms of silicon in natural waters by atomic absorption spectrometry with electrical atomization and spectrophotometry .: dis. ... Cand. chem. Sciences: 02.00.02 / M.G. Kambalina. - Tomsk, 2015. –139 p. - Bibliography: p. 101-125.

2IL

Cold gas-phase spectroscopy: a case study of hypervalent carbon compounds

Satoru Muramatsu

[1] Department of Chemistry, Graduate School of Advanced Science and Engineering, Hiroshima Univ.

A hypervalent carbon compound having a penta-coordinated carbon atom is typically seen as a transition state of S_N2 reactions (Figure 1a), and thus experimental studies of its structure have been receiving great attention. Yamamoto and coworkers have succeeded in chemical synthesis of "stable" penta-coordinated carbon compounds[1] (e.g. compound **1** in Figure 1b), although the structural characterization just relied on X-ray diffraction analyses of a single crystal. It is highly desired (1) to examine intrinsic structure of the compounds by isolation in the gas phase and (2) to spectroscopically characterize the hypervalent nature.

To these ends, I herein investigated electronic and geometrical structures of **1** and **2**, with different ligands, by means of photodissociation spectroscopy (PDS)[2] under the cold gas-phase condition, with the aid of ion mobility mass spectrometry (IMMS) measurements.[3] Penta-coordinated (hypervalent) structure of **1** was dominantly identified by both of PDS and IMMS. On the other hand, coexistence of penta- and tetra-coordinated (non-hypervalent) isomers was revealed for compound **2** in the gas phase; it is in sharp contrast to its exclusive tetra-coordinated structure in a crystal (Figure 1c). The cause of such difference will be discussed on the basis of the relative stabilities, to shed new light on the origin of the hypervalent structure.

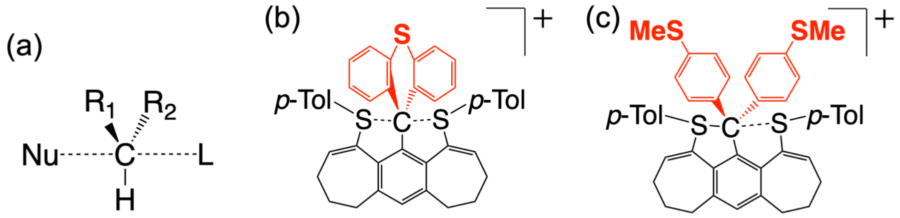

1; penta-coordinated **2**; tetra-coordinated

(In single crystal)

Figure 1: (a) Transition state of S_N2 reaction. (b, c) Schematic structures of target compounds in a single crystal. Ligands are indicated in red. *p*-Tol indicates a *para*-tolyl ($–C_6H_4–CH_3$) group.

Acknowledgments: I am grateful to Prof. Yoshiya Inokuchi (Hiroshima Univ.) for giving me the opportunity to do this work. I thank Prof. Y. Yamamoto (Hiroshima Univ.) for providing the samples, and Dr. K. Ohshimo and Prof. F. Misaizu (Tohoku Univ.) for IMMS measurements.

References: [1] Y. Yamamoto et al., *J. Am. Chem. Soc.* **121**, 10644 (1999). [2] Y. Inokuchi et al., *J. Phys. Chem. A* **119**, 8512 (2015). [3] K. Ohshimo et al., *Phys. Chem. Chem. Phys.* **22**, 8164 (2020).